ACS NANO

www.acsnano.org

DOI: 10.1021/acsnano.6b01752
ACS Nano 2016, 10, 4816−4827

ARTICLE

Strong and Tough Layered Nanocomposites with Buried Interfaces

Ke Chen, Xuke Tang, Yonghai Yue,* Hewei Zhao, and Lin Guo*

Key Laboratory of Bio-Inspired Smart Interfacial Science and Technology of Ministry of Education, Beijing Key Laboratory of Bio-inspired Energy Materials and Devices, School of Chemistry and Environment, Beihang University, Beijing 100191, P. R. China

Presented by,

Sritama Mukherjee
01.04.2017

Nacre : mother of pearl

Figure 1. Hierarchical structure feature, phase dispersion, and micromechanical behavior in natural nacre.
(a) Schematic drawing of hierarchical structure (five levels) of natural nacre from nano, micro, to structural length scales. At the nanoscale level, show are the components including aragonite crystals, β -chitin fibrils, analogous silk protein, and other inorganic minerals. At coarser levels, shown is the model of the organic membrane/matrix between platelets; at the microscale levels, shown is the mechanism of growth of nacreous platelets and sheet nacre. On the largest length scales is the apparent shape of the bivalve. (b) TEM image of nacre nanograins.
(c) The selected area diffraction pattern corresponding to selected area [rectangular area G in (b)], exhibiting the polycrystalline characteristic pattern of the aragonite.
(d) HRTEM image of nacre nanograins, showing the complex grain and phase boundary. (e) The fast Fourier transform (FFT) pattern corresponding selected area H in (d). Some nanocrystals are outlined with dark yellowed dashed lines and the interplanar distances of
(021), (012), (200), (112), and (113) planes of the aragonite are observed. (f) ICP-MS element analysis and SEM-EDS element mapping of nacre (bivalve pearl oyster shell), indicating various metal elements/minerals. (g and h) The contour maps of E_c and H_c dispersion on the nacre plane corresponding to the image (b) of an array, respectively, indicating the nonuniform mechanical dispersion (P'_{max} = 800 μN)

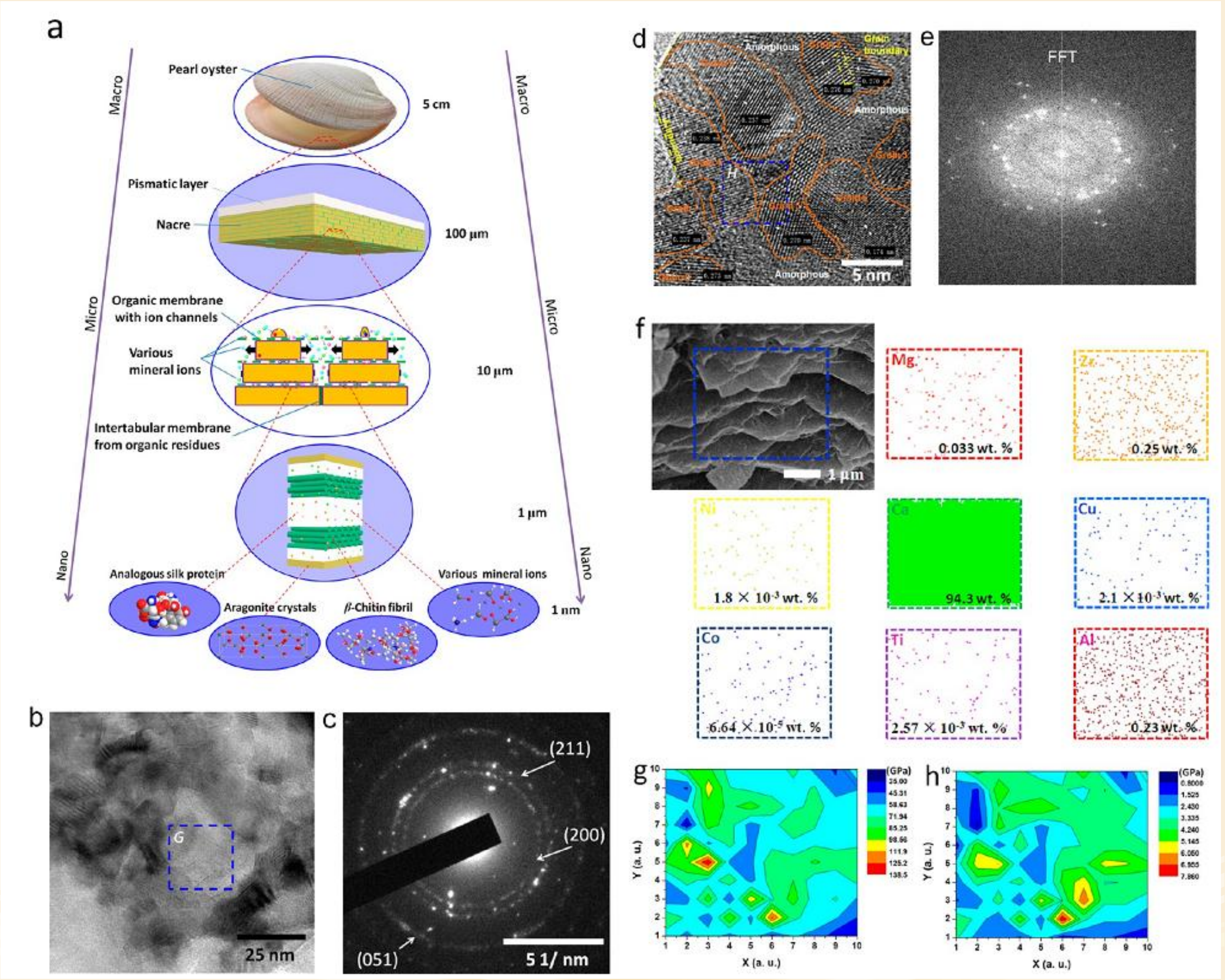

Background:

- On the basis of the nacre's structure, most of the bioinspired layered materials are fabricated primarily by mimicking the ordered microstructures and simple interfaces to achieve combination of stiffness, strength and toughness.

- The mechanical property and the hierarchical structures of natural nacre has been well correlated.

- Biomineralization process: besides the predominant mineral (CaCO3) and organic (polysaccharides and proteins) components, biological organisms from mollusks can guide some small amount of other minerals/ions (e.g., Mg2+, Al2O3, ZrO2, TiO2, CaO, and so on) to form the layered composite materials; these minerals/ ions interact with organic matrix to form buried inorganic −organic complex interfaces at multiple hierarchical levels, referring to the mineralized platelets and organic matrix.

- Notion: High strength => toughening mechanism => crack deflection => tortuous path => dissipates more energy.

- Mechanical enhancement due to other structural / component factors have been ignored.

- **Question asked: Do buried ions/minerals enhance intrinsic toughness?**

Objective:

- Fabricate artificial nacre (M^{n+}-GO/CMC) with high strength and toughness . (i.e. Fabrication of Pure GO, CMC, GO/CMC, and M^{n+}-GO/CMC Composite Papers (M^{n+}: Mg^{2+}, ZrO^{2+}, Ni^{2+}, Ca^{2+}, Cu^{2+}, Co^{2+}, TiO^{2+}, Al^{3+})

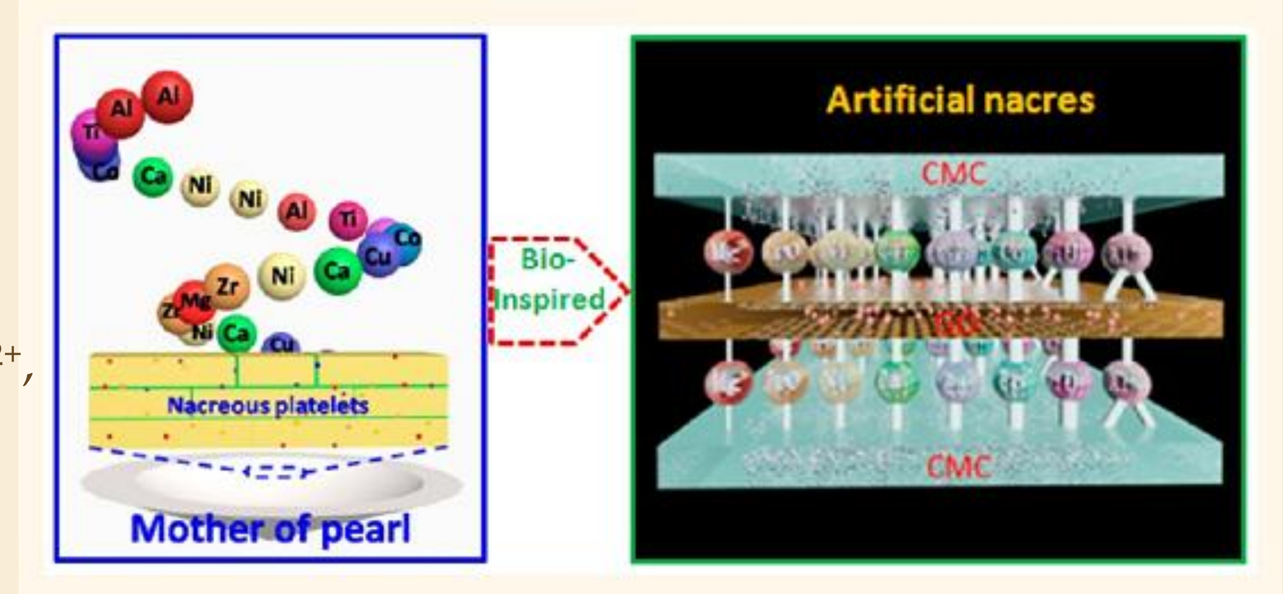

- Measurements of macro –micromechanical properties

GO/CMC Composite dispersion filtered-VAF

6.56 vol% GO in wet GO/CMC composite paper

Add aq. M^{n2+}solution (20-100mL, 0.05 mM sol)

After filtration, specimens were air dried

Characterization

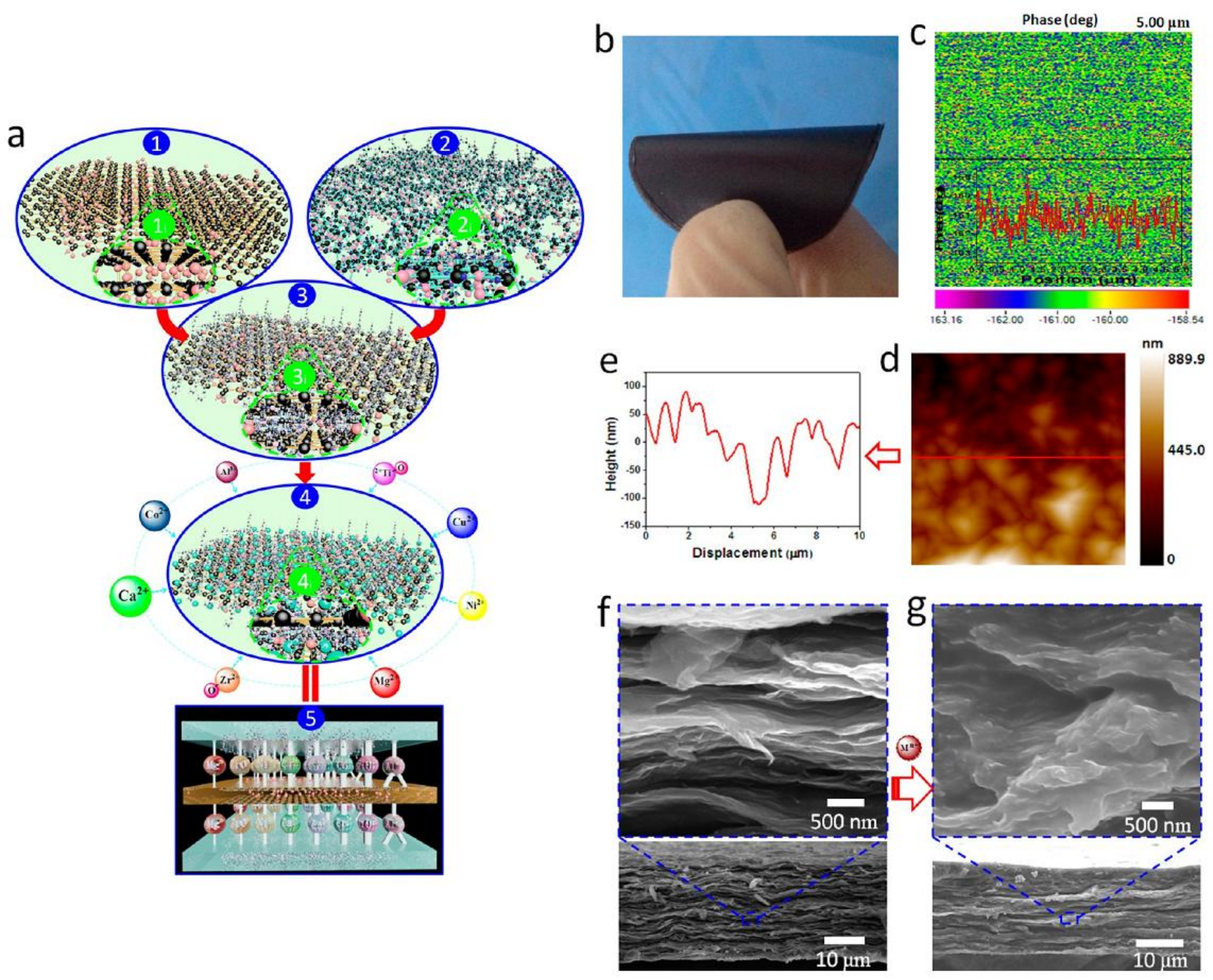

Figure 2. Design strategy depicting the control of structural self-organization and microstructural features for our artifi cial nacres.

(a) Design fabrication process describing the strengthening and toughening control at multiple scales of structural self-assembly based on individual GO nanosheets (①), renewable CMC (②), and different cationic metals/oxygen-contained metals (M^{n+}), and interfacial strengthening and toughening strategy. Self-assembling of the staggered layered structural features is obtained by VAF (③). The chemically strong cross-linking interactions between the oxygen-containing groups of GO nanosheets/CMC polymers and M^{n+} ions (④ and ⑤).

(b) Digital image of a brown free-standing paper (e.g., Al^{3+}-GO/CMC), showing a good flexibility. Within 10.0 μm × 10.0 μm.

(c) The map of the uniform phase distribution (e.g., Al^{3+}-reinforced) under 100 μN force by using the nanoindentation within 5.00 μm × 5.00 μm surface area. (d) Tapping mode AFM height images, showing the relative flattening of nanocopic asperities on the plane of the sample (b)-roughness=135 nm. (e) Height profile of the red line in part d. (f and g) Cross section morphology of the layered GO/CMC composite (f) and a typical artificial nacre paper (Al^{3+}-reinforced)
(g), indicating a layered arrangement: bottom to top, low- and high- resolution SEM images, respectively.

Characterization

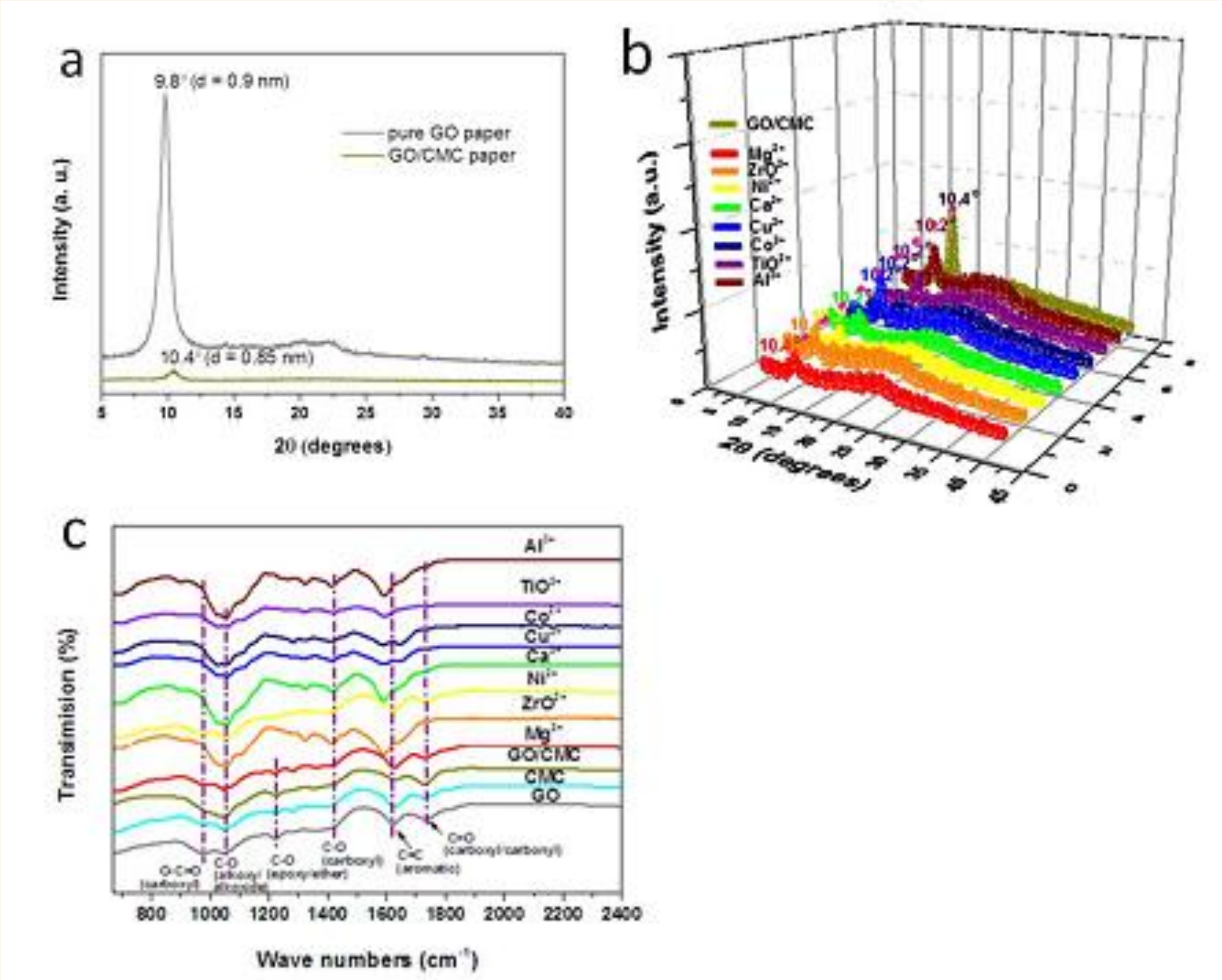

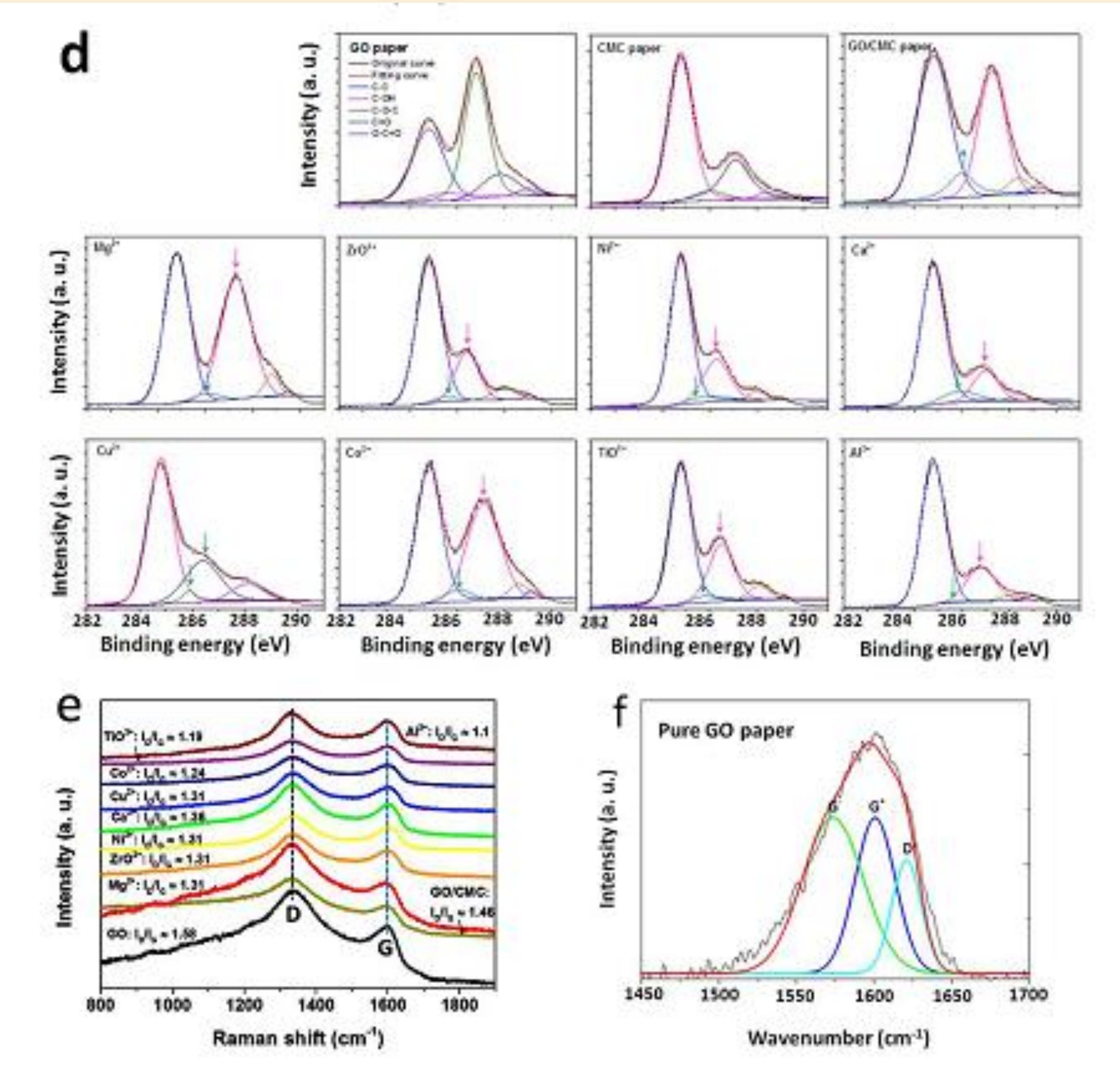

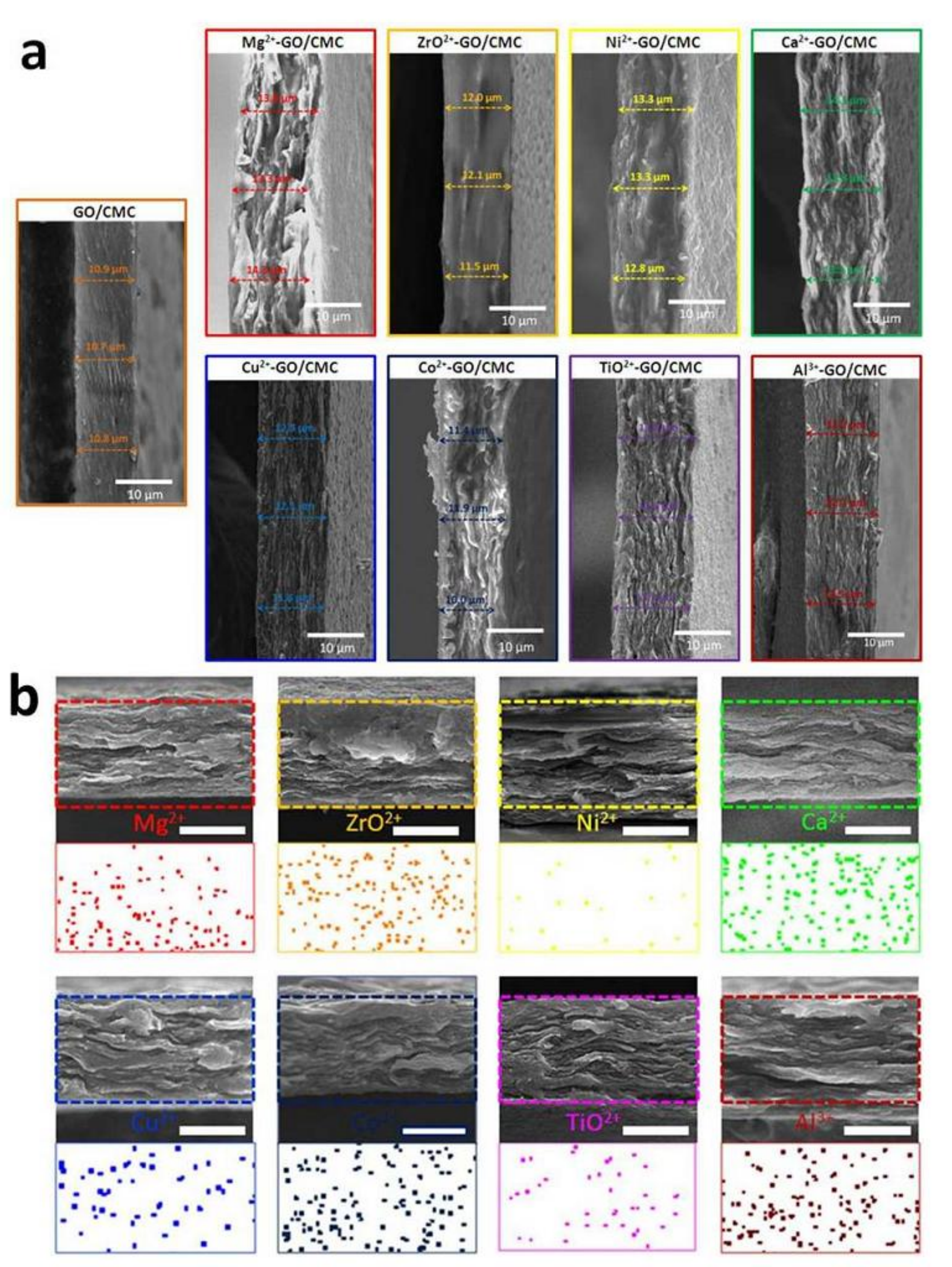

Figure S4. The thickness change and element dispersions in artificial nacres after incorporating M^{n+} ions. (a) The comparison of the thickness change between GO/CMC and M^{n+}-GO/CMC composite papers. Thickness difference: 1.0-2.5 um

(b) SEM-EDS element mapping of M^{n+}-GO/CMC composite papers. Scale bar, 5 μm

Macro-microscopic behaviors

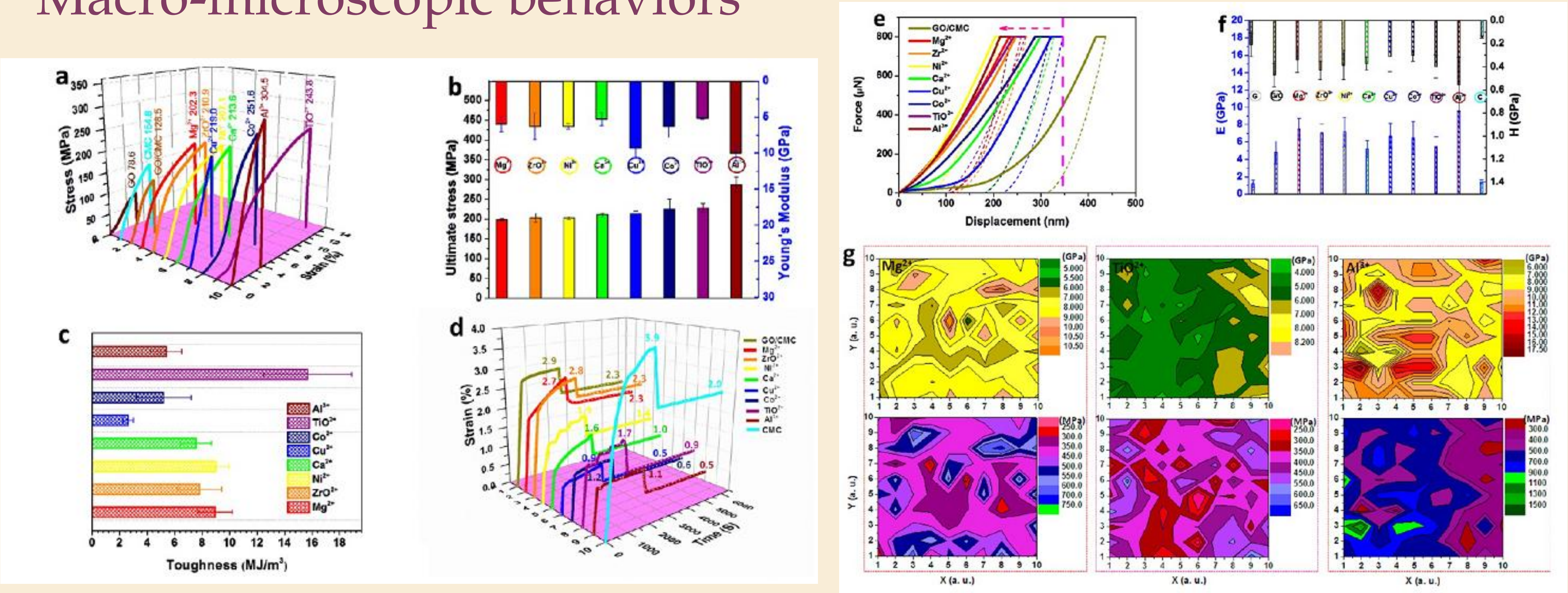

Figure 3. Macro − microscopic mechanical behaviors of artificial nacres. (a) Representative stress − strain data from tensile test. (b) Graphical comparison of the ultimate stress (σ_{g-c}) and Young's modulus (E_{g-c}). (c) Graphical comparison of the toughness (W_{g-c}). (d) Typical creep and recovery curves. (e) Typical load−displacement curves with h_{max} = 130 −450 nm performed in the load of 800 μN (Nanoindentation points, n = 5). (f) Graphical comparison of the calculated Young's modulus (E'_{g-c}) and hardness (H'_{g-c}) based on Oliver-Pharr analysis as a function of maximum load (P'_{max}) from 150 to 1000 μN (n > 6). (Note: G = GO, C = CMC, G/C = GO/CMC). (g) The typical contour maps of E'_{g-c} (top) and H'_{g-c} (bottom) dispersion on the composite papers plane within 15 μm × 15 μm (e.g., Mg^{2+}, TiO^{2+}, Al^{3+}, P'_{max} = 800 μN)

Materials	Adding ions content (μL)	Experimental content (wt. %)	$\sigma_{g\text{-}c}$ (Mpa)	$W_{g\text{-}c}$ ($MJ \cdot m^{-3}$)	$E_{g\text{-}c}$ (GPa)
GO			87.9 ± 14.4	2.4 ± 1.5	4.5 ± 0.2
CMC	-	-	138.2 ± 19.4	3.9 ± 1.1	4.0 ± 1.0
GO/CMC	-	-	129.5 ± 7.9	1.9 ± 0.6	6.9 ± 0.8
Mg^{2+}	40	0.52	198.2 ± 2.9	9.0 ± 1.3	5.9 ± 1.0
ZrO^{2+}	20	0.98	202.0 ± 11.6	7.8 ± 1.6	6.3 ± 1.8
Ni^{2+}	70	1.10	202.0 ± 3.7	9.00 ±1.0	6.4 ± 0.4
Ca^{2+}	60	1.50	210.6 ± 5.2	7.6 ± 1.1	5.3 ± 0.9
Cu^{2+}	40	0.47	213.2 ± 6.1	2.6 ± 0.4	9.3 ± 1.4
Cu^{2+}	60	0.58	191.1 ± 7.5	9.7 ± 0.5	5.5 ± 0.5
Co^{2+}	80	0.72	225.2 ± 25.4	5.2 ± 2.0	6.3 ± 1.5
TiO^{2+}	80	0.70	228.2 ± 11.0	15.7 ± 3.2	5.1 ± 0.2
Al^{3+}	60	0.22	286.4 ± 19.4	5.4 ± 1.1	10.0 ± 1.1

toughness ($W_{g\text{-}c}$).

Young's modulus ($E'_{g\text{-}c}$

hardness ($H'_{g\text{-}c}$)

stress ($\sigma_{g\text{-}c}$)

Comparison of mechanical properties of M^{n+}-GO/CMC with neat GO, CMC, and GO/CMC paper

Nanoindentation studies

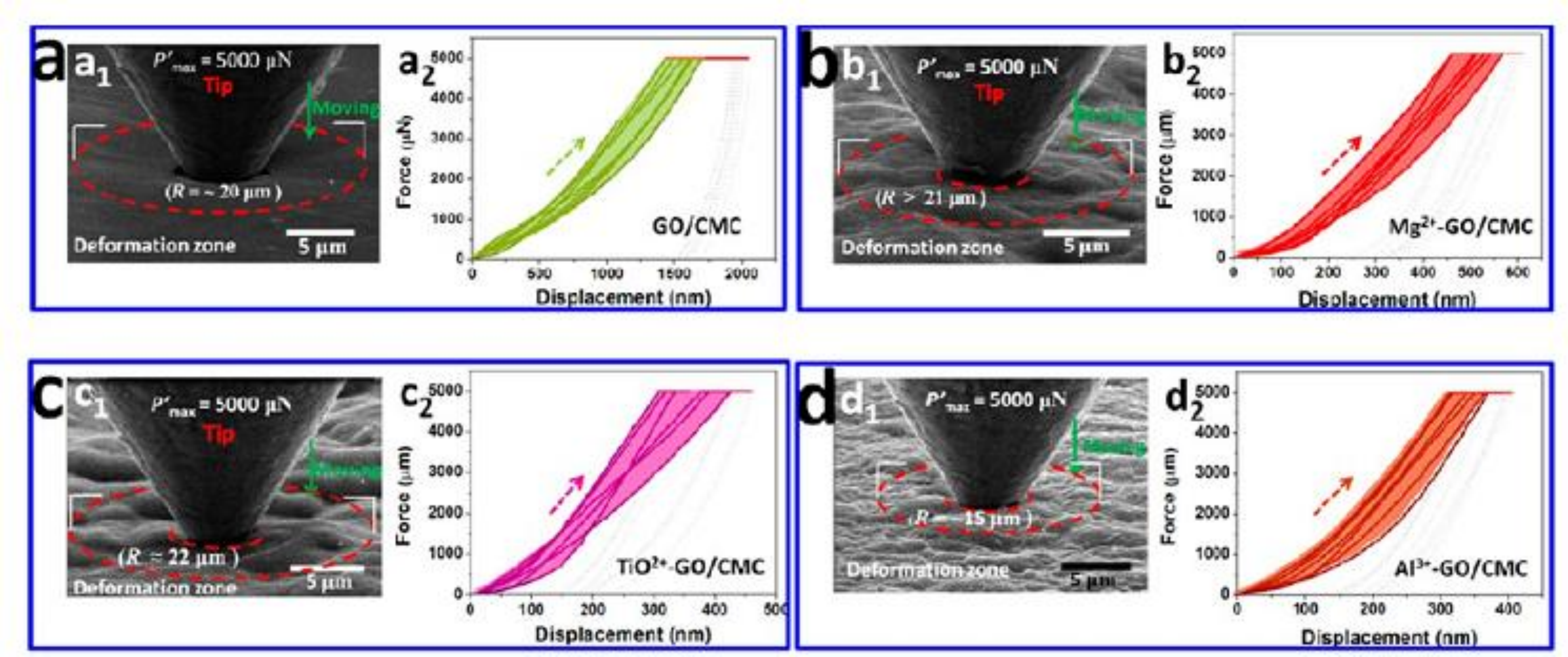

Comparison of the microscale deformation and multiple individual load − displacement curves (Figure 4a$_2$ −d$_2$) for GO/CMC, Mg^{2+}-, TiO^{2+}-, and Al^{3+}-GO/CMC

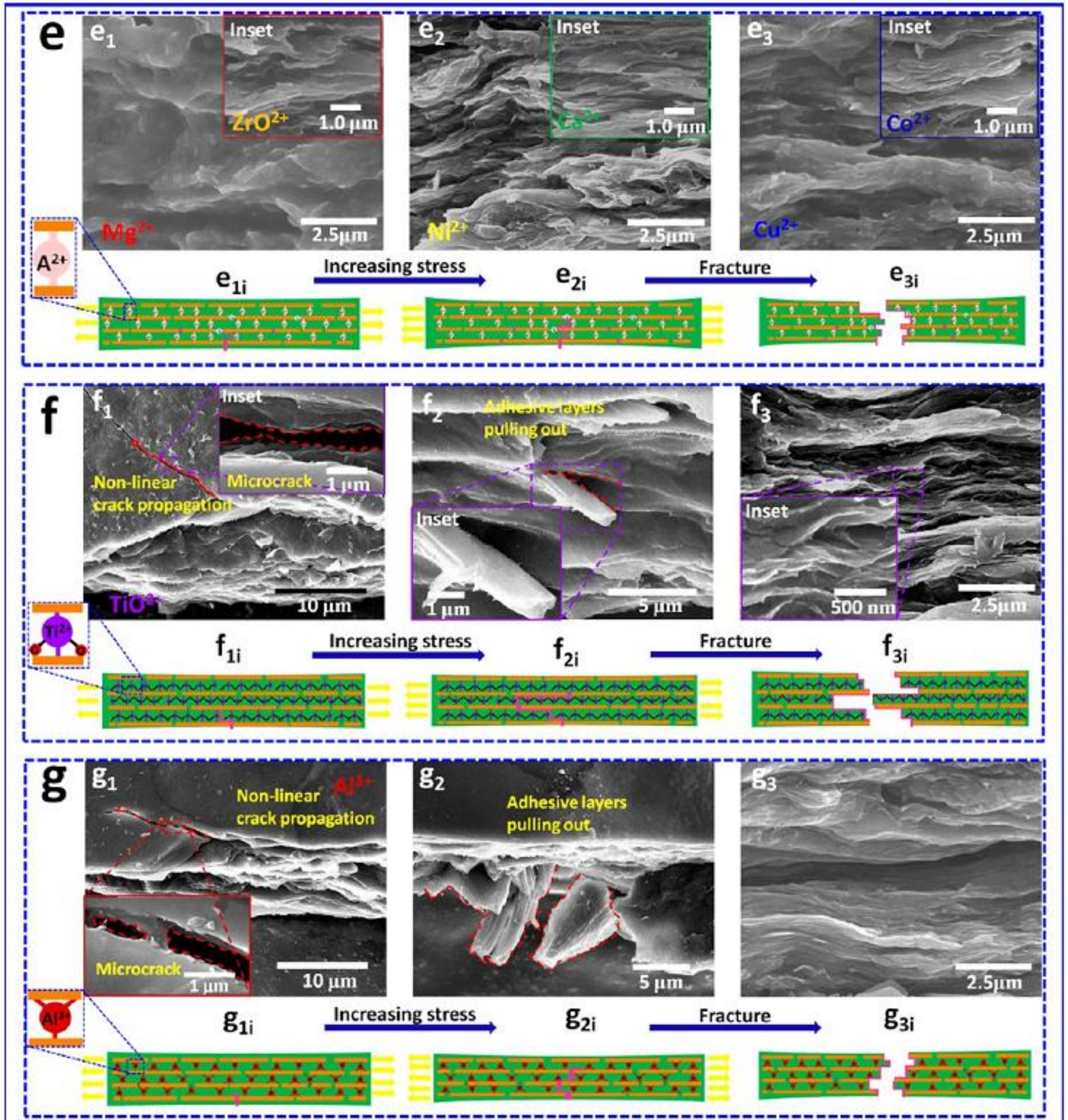
e
e1
Inset
ZrO2+
1.0 μm
Mg2+
2.5μm
e2
Inset
1.0 μm
Ni2+
2.5μm
e3
Inset
Co2+
1.0 μm
Cu2+
2.5μm
A2+
e1i
Increasing stress
e2i
Fracture
e3i
f
f1
Inset
Microcrack
1 μm
Non-linear crack propagation
10 μm
f2
Adhesive layers pulling out
Inset
1 μm
5 μm
f3
Inset
500 nm
2.5μm
Ti2+
f1i
Increasing stress
f2i
Fracture
f3i
g
g1
Non-linear crack propagation
Al3+
Microcrack
1 μm
10 μm
g2
Adhesive layers pulling out
5 μm
g3
2.5μm
Al3+
g1i
Increasing stress
g2i
Fracture
g3i

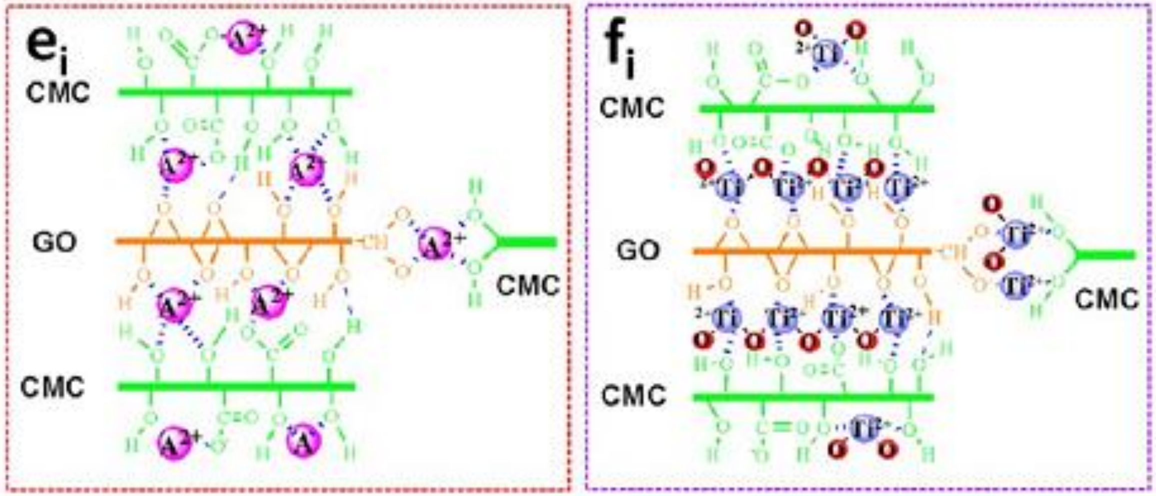
ei
CMC
GO
CMC
CMC
fi
CMC
GO
CMC
CMC

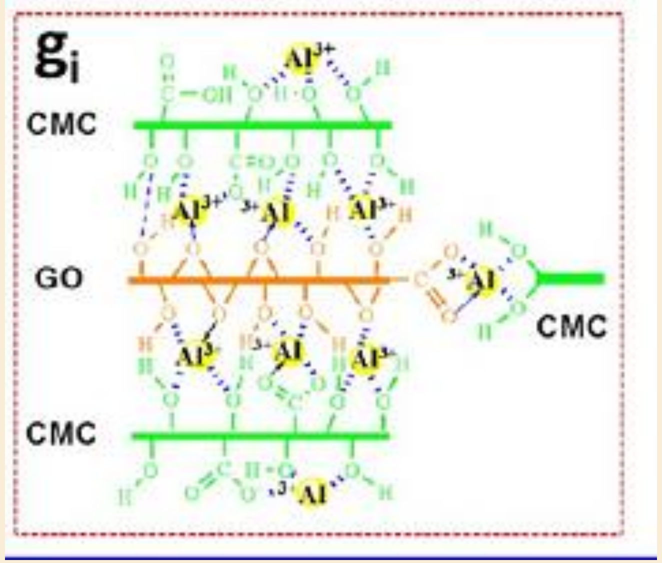
gi
CMC
CMC
GO
CMC

3 crack models to depict synergistic reinforcing effect

(I) Initially, subjected to stress: a deflected microcrack caused by a GO nanosheet encounters the chemically cross-linking sites. For A^{2+}, a relatively large slip with slight deflection happened; for TiO^{2+} and M^{3+} (e.g., Al^{3+}), the relatively large deflected microcrack with a relatively small slip can be caused by the strongest load transfer capability of the Al −O bonding and the increase of the friction force originated from thecomplex chains (−Ti−O −Ti−), together with chemical crosslinking sites on the GO/CMC interfaces, respectively.

(ii) Increasing stress: the chemical cross-linking sites bridges the microcrack. The cross-linking M^{n+} ions can effectively restrict the relative slip of these two parts (strain hardening). For TiO^{2+}, the complex chains could improve the sliding distance of adjacent GO nanosheets obviously. The enhanced stress was transferred rapidly to a vicinal one along the interfacial layer, which subsequently motivated the potential loosening/break of adjacent multiple adhesive layers.

(iii) Fracture: such crack deflection, strain hardening and motivation of the potential loosening/break of multiple adjacent adhesive layers were accumulated step by step until the failure. In this case, energy dissipation by sacrificing cooperative bonding and sliding of GO nanosheets and CMC layers result in the synergistic reinforced strategy.

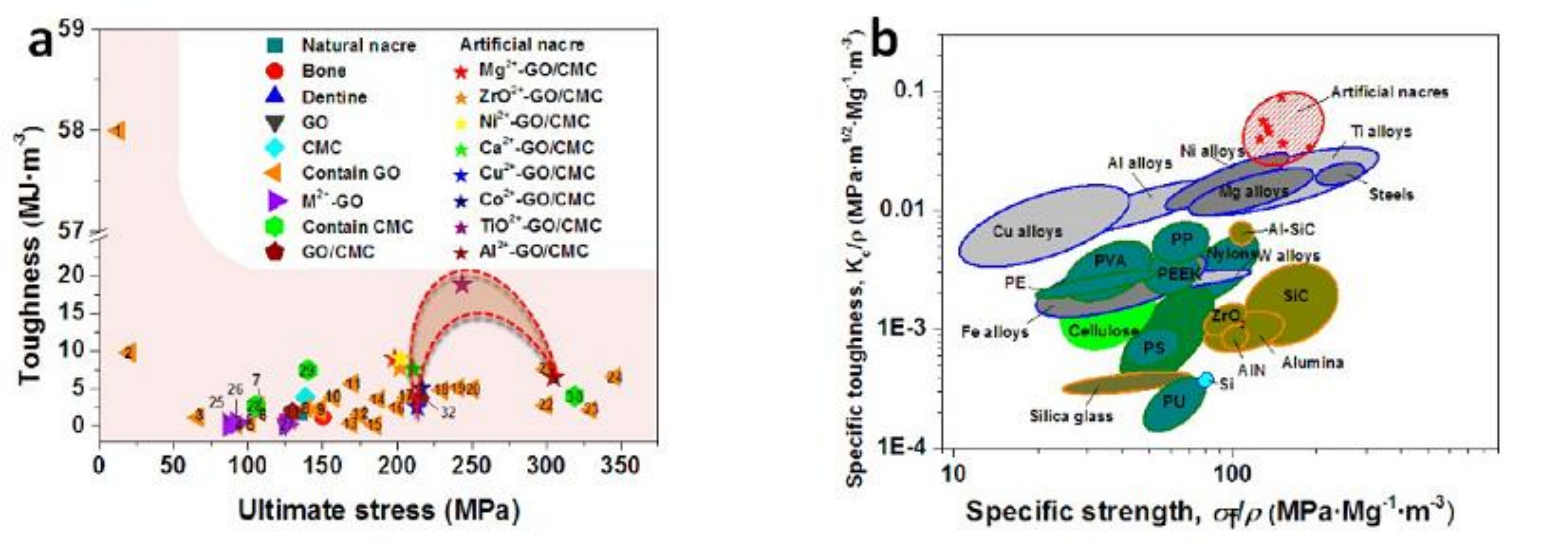

Figure 5. Comparison of these related materials' performance. (a) Toughness versus tensile strength for several natural materials, GO- and CMC-related film/papers. The stars represent our artificial nacres. The references are shown as follow: (Nacre,[8] Bone,[41] Dentine,[42] 1, GO/PU (Song, 2012);[33] 2, GO/PCL (Inoue, 2008);[46] 3, GO/PS (Wu, 2015);[47] 4, GO/PPA (Ruoff, 2009);[48] 5, GO/GA (Zhang, 2011);[37] 6, GO/(PAH −PSS) (Tsukruk, 2010;,[49] 7, GO/PCDO (Cheng, 2013);[50] 8, GO/PAH (Gun'ko, 2010);[51] 9, GO/CS (Yan, 2011);[52] 10, GO/PVA (Maser, 2013);[53] 11, GO/MoS_2-TPU (Cheng, 2015); [54] 12, GO/NCCA (Namazi, 2014);[55] 13, Fe^{3+}-GO/TA (Xu, 2014);[56] 14, GO/Borate (Nguyen, 2011);[4] 15, GO/PAD (Cheng, 2014);[38] 16, GO/PBI (Wang, 2013);[57] 17, GO/$PAPB_x$ (Shi, 2014);[58] 18, GO/PVP (Shi, 2015);[59] 19, GO/G_4NH_2 (Shi, 2015);[59] 20, GO/PEI (Shi, 2015);[59] 21, GO/CS (Shi, 2015);[59] 22, GO/RGO-Silk (Tsukruk, 2013);[60] 23, GO/SF (Tsukruk, 2013);[9] 24, GO/CS (Cheng, 2015);[61] 25, Mg^{2+}/GO (Ruoff, 2008);[35] 26, Fe^{3+}/GO (Xu, 2014);[56] 27, Ca^{2+}/GO (Ruoff, 2008);[35] 28, GO/CMC/SA (Park, 2014);[62] 29, CMC/UFOs (Inagamov, 2011);[63] 30, CMC/MTM (Walther, 2013);[26] 31, GO/CMC (Guo, 2015); 32, GO/CMC (Shi, 2015).[59] (b) Ashby diagram of specific strength versus specific toughness of a range of engineering and natural materials.[43] The red stars in red circle refer to our artificial nacres. Fracture toughness $K_c \approx (E' \cdot J_{g\text{-}c})^{1/2}$ (MPa ·$m^{1/2}$), where K_c is the fracture toughness, $E'_{g\text{-}c}$ is the Young's modulus (GPa), and $J_{g\text{-}c}$ (kJ ·m^{-2}) is the toughness of our artificial nacres, which is equal to the essential work (w_e) (according to Essential Work of Fracture (EWF) approach,[64]

Conclusion

- Inspired by the role of various minerals formed buried interfaces in nacre, a typical kind of artificial nacre (M^{n+}-GO/CMC) with high strength and toughness has been successfully fabricated.
- The measurements of macro −micromechanical properties show that the chemical cross-linking reactions between M^{n+} ions and oxygen-containing groups of the two components can dramatically strengthen/toughen the GO/CMC interfaces, which significantly restrict the relative slip of between GO nanosheets and CMC layers, resulting in a great improvement of strength and toughness.
- However, owing to the differences in the bonding styles and different bonding energies of the M −O bonds, the reinforcing strategies of different types of M^{n+} ions reflect the diverse increases in mechanical properties.
- More importantly, this special reinforcing effect opens a promising route to strengthen and toughen materials, investigation provides new opportunities in developing the bioinspired composite materials with superior mechanical properties for a wide range of applications, such as aerospace, artificial muscles, tissue engineering, and wearable electronic devices.

Thanks.